Luqi Wang · Yueping Yin · Zhihua Zhang · Bolin Huang · Yunjie Wei · Peng Zhao · Mingjun Hu

Stability analysis of the Xinlu Village landslide (Chongqing, China) and the influence of rainfall

Abstract On June 28, 2016, a landslide occurred in Xinlu Village, Qijiang District, Chongqing, China. The landslide volume was 854,200 m³. Exposed to continuous rainfall, the rocky part of the trailing edge slipped first, and then the soil part of the leading edge was pushed downward. Numerical simulations were used to analyze the formation characteristics of the landslide and to predict the stability of the landslide after the slip. In order to ensure the accuracy and rationality of numerical calculation, we used field surveys, laboratory tests, and back-calculation to restore the typical sections, determine the relevant mechanical parameters, and control boundary conditions. The displacement, stress, effective plastic strain distribution, and safety factor, obtained by numerical calculation, were compared to examine the action of rainfall. According to the evaluation of landslide stability and numerical calculation results, the Xinlu Village landslide remained in a peristaltic stage after the initial overall sliding, and additional sliding could occur under storm conditions.

Keywords Rainfall-induced landslide · Formation mechanism · Slumping slide · Numerical simulation

Introduction

Landslides cause significant casualties and economic losses every year. One important cause of landslides is rainfall, and rainfall-induced landslides have always been the focus of landslide research (Crosta and Frattini 2008; Liao et al. 2010; Clague and Stead 2012; Yin et al. 2016; Wang et al. 2019).

In recent decades, with the development of computer technology and related numerical analysis software, numerical simulation has become one of the most popular methods for analyzing the formation mechanism and stability of rainfall-induced landslides (Rahimi et al. 2011; Ren et al. 2016; Gao et al. 2017). Compared with theoretical research and model testing (Ling et al. 2010; Wu 2015; Irfan et al. 2017), the advantage of numerical simulation is that it can simulate the formation characteristics of landslides under various conditions through reasonable numerical model analyses. This facilitates understanding of the failure mechanism of landslides, the evaluation of stability, and management for disaster prevention (Wen et al. 2018). However, the accuracy of numerical simulation when studying rainfall-induced landslides depends not only on the comprehensive analysis of geological conditions (Hungr and Evans 2004; Li et al. 2018) but also on the type of mechanical model, the boundary conditions, and selection of the mechanical parameters (Zhang et al. 2015; Cheng et al. 2018; Lin et al. 2018).

The Xinlu Village landslide studied here slipped under the effect of continuous heavy rainfall in a short time. The trailing edge of the landslide was rock, and the leading edge was soil. In addition, a secondary disaster of debris flow was caused by landslides in this study area. Because the failure mechanism of the landslide was complicated, field surveys, laboratory tests, and back-calculation were used to ensure the accuracy and rationality of numerical calculation in this paper. Furthermore, by comparing

the numerical calculation results under different conditions, the influence of rainfall on the landslide and the prediction of trends were analyzed.

Overview of the landslide

From June 26 to June 28, 2016, the study area experienced continuous heavy rain. The cumulative rainfall was approximately 160 mm, which caused a large number of landslides and collapses. Among these, the Xinlu Village landslide (106° 44′ 50″ E, 28° 43′ 36″ N; Fig. 1) closed the railway and caused the collapse of four houses. It threatened multiple residences on the front edge of the landslide and endangered rescue workers who were repairing the closed Sichuan–Guizhou railway. The landslide was located on the right bank of the Songkan River and above the Leihoudong tunnel of the Sichuan–Guizhou railway. The landslide had a length of 452.6 to 514.2 m, a horizontal width of 108.1–130.4 m, with an area of 56,200 m², a thickness of 5.5–35.1 m (mean thickness = 15.3 m), and a volume of approximately 854,200 m³. It was a medium-sized landslide, and the main slide direction was approximately 270°.

Two groups of structural fractures developed in the study area. The representative occurrence of the first group of structural fractures was 62°∠86°, with a spacing of 1 to 3 m, an opening from 1 to 5 mm, no filling, and an extension length from 2 to 10 m. The representative occurrence of the second group of structural fractures was 160°∠75°, with a spacing of 1 to 5 m, an opening from 1 to 5 mm, no filling, and an extension length from 2 to 15 m.

The landslide was located on the gentle slope of the low mountain valley formed by the Songkan River. The main strata of the landslide were artificial deposits (Q_4^{ml}), landslide deposits (Q_4^{del}), residual slope deposits ($Q_4^{el + dl}$), and collapsed deposits (Q_4^{col}) of the Quaternary Holocene. The exposed bedrock was mainly mudstone and sandstone of the Mid-Jurassic Shaximiao Formation (J_{2s}).

Human engineering activities in the landslide area mainly involved the construction of the Sichuan–Guizhou railway at the leading edge of the slope, resulting in the excavation of the toe of the slope, which provided spatial conditions for a landslide.

Deformation characteristics of the landslide

At 7:30 p.m. on June 28, 2016, overall slippage of the Xinlu Village landslide occurred. The sliding distance of the rock mass on the trailing edge was approximately 30 m, forming a tension crack slot. The rear part of the landslide was a rocky slope, and the middle-front part was a soil slope, which was an early Caifengyan landslide.

After the landslide slip, the rock debris in the rear part of the landslide fragmented, and the central and frontal areas were densely split. There were several deformation cracks in the northern frontal residential area.

Nine sections and 17 drill holes were used to analyze the formation characteristics of the landslide (Fig. 2). The field investigation showed that the rear sliding mass was the debris of mudstone after disintegration, and the middle-front sliding mass was mainly silty clay and gravel. The sliding zone of the middle-
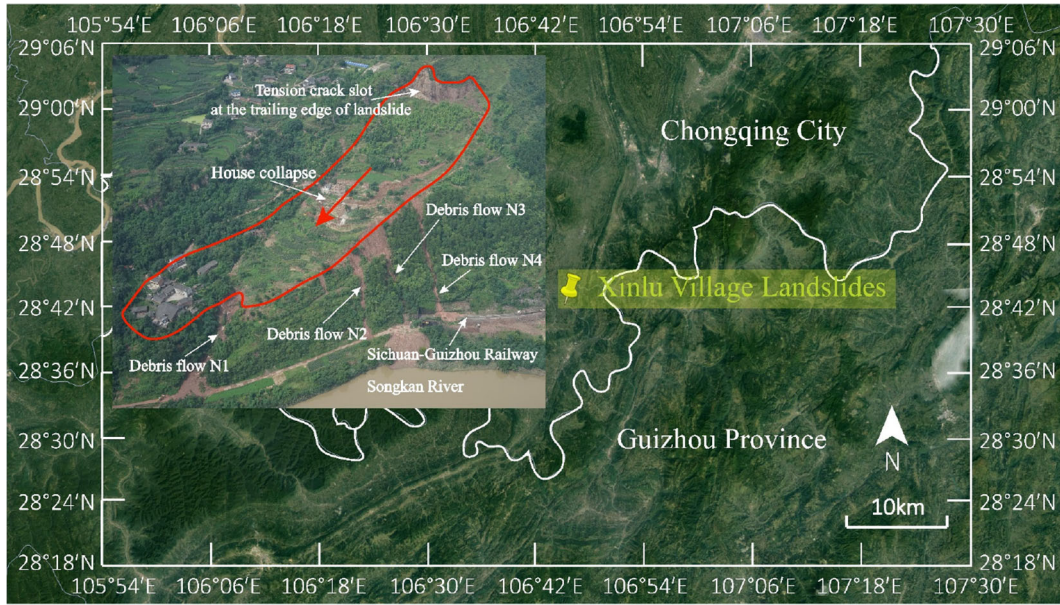
Fig. 1 Location of the Xinlu Village landslide

front soil part was breccia, and the sliding zone of the rocky part was the weak muddy interlayer between rock layers. The slide bed was mainly sandstone of the Mid-Jurassic Shaximiao Formation (J_{2s}). Based on the deformation of the landslide and the developmental characteristics of the surface cracks, the landslide was divided into a rear slip progressive area (Area I), a mid-front extrusion area (Area II), and a north-front extrusion deformed area (Area III). Among these, Area II was divided into the central extrusion bulge sliding subzone (Area II_1), the south-lateral extrusion loose slump subzone (Area II_2), and the front extrusion loose slump subzone (Area II_3) (Zhao et al. 2018; Fig. 2).

Failure mode of the landslide
Under the action of the high fissure-water pressure and the sliding-surface-lift pressure caused by continuous rainfall infiltration, the rocky part on the trailing edge of the landslide slipped first. After

being pushed and squeezed by the rear rocky part of the landslide, the front original Caifengyan landslide could not provide sufficient anti-sliding force and directly slipped. Therefore, the failure mode of this landslide was defined as a slumping slide.

According to the site investigation, the deformation of the original Caifengyan landslide gradually developed from front to back, and the deformation of the front edge was more intense. Therefore, the failure mode of the original Caifengyan landslide was a loose slide.

The steep slopes on the south and at the front of the landslide were weak stress areas. After silty clay and gravel were squeezed, they were extruded directly on the steep slope. The large number of deformation cracks that developed provided paths for the infiltration of rainfall. During the rainy season, the soil could quickly become saturated, and the shear strength would be reduced. Thus, an arc-shaped instability occurred, and a secondary disaster of debris flow formed along the steep slope.
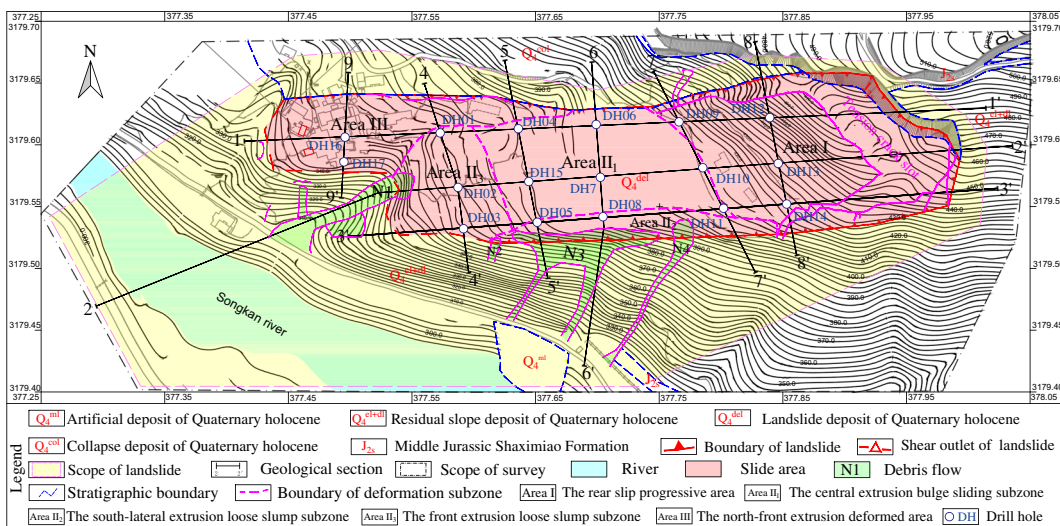

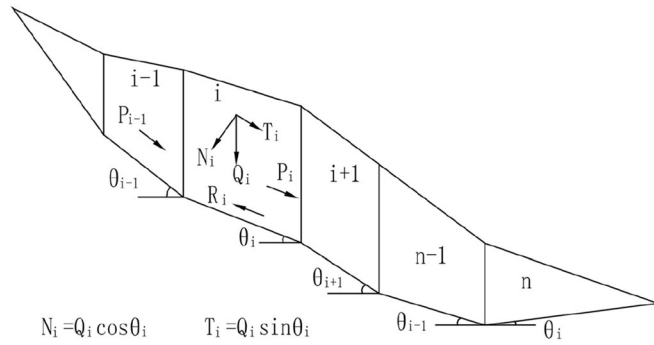**Fig. 2** Overview of the Xinlu Village landslide

Fig. 3 Method for calculation of the transfer coefficient

$$N_i = Q_i \cos\theta_i \qquad T_i = Q_i \sin\theta_i$$

The Xinlu Village landslide was in a peristaltic stage after the overall sliding and was in an unstable state. After heavy or continuous rainfall, it is possible that the landslide will slip again. The sliding mass that had been squeezed at the front and southern edge of the landslide may partially collapse.

Selection of geotechnical parameters and the establishment of a numerical model

Based on a laboratory test, the mechanical parameters of the sliding zone were back-calculated, and the typical section before the slip was restored. The 1-1′ section was taken as an example to carry out relevant calculations.

Back-calculation model and method

The rocky part of the trailing edge underwent plane sliding, and the sliding zone of the middle-front soil part was the geotechnical interface, which was presented as a polyline. Limit equilibrium theory and the polyline-type sliding transfer coefficient method (Technical code for building slope engineering 2013; Li 2016; Fig. 3) were used to calculate the stability of the landslide as a whole as well as the mid-front of the original Caifengyan landslide.

The formulas used in the back-calculation model are as follows:

$$F_s = \frac{\sum_{i=1}^{n-1}\left(R_i \prod_{j=i}^{n-1}\psi_j\right) + R_n}{\sum_{i=1}^{n-1}\left(T_i \prod_{j=i}^{n-1}\psi_j\right) + T_n} \tag{1}$$

$$R_i = [W_i\cos\alpha_i - Q_i\sin\alpha_i + D_i\sin(\beta_i-\alpha_i) - V\sin\alpha_i - U_i]\tan\phi_i + c_i l_i \tag{2}$$

$$T_i = W_i\sin\alpha_i + Q_i\cos\alpha_i + D_i\cos(\beta_i-\alpha_i) + V\cos\alpha_i \tag{3}$$

$$\psi_j = \cos(\alpha_i-\alpha_{i+1}) - \sin(\alpha_i-\alpha_{i+1})\tan\phi_{i+1} \tag{4}$$

$$\prod_{j=i}^{n-1}\psi_j = \psi_i\psi_{i+1}\psi_{i+2}\psi_{i+3}\ldots\psi_{n-1} \tag{5}$$

$$D_i = \gamma_w h_i l_i \cos\alpha_i \beta_i \tag{6}$$

$$V = \frac{1}{2}\gamma_w h_w^2 \tag{7}$$

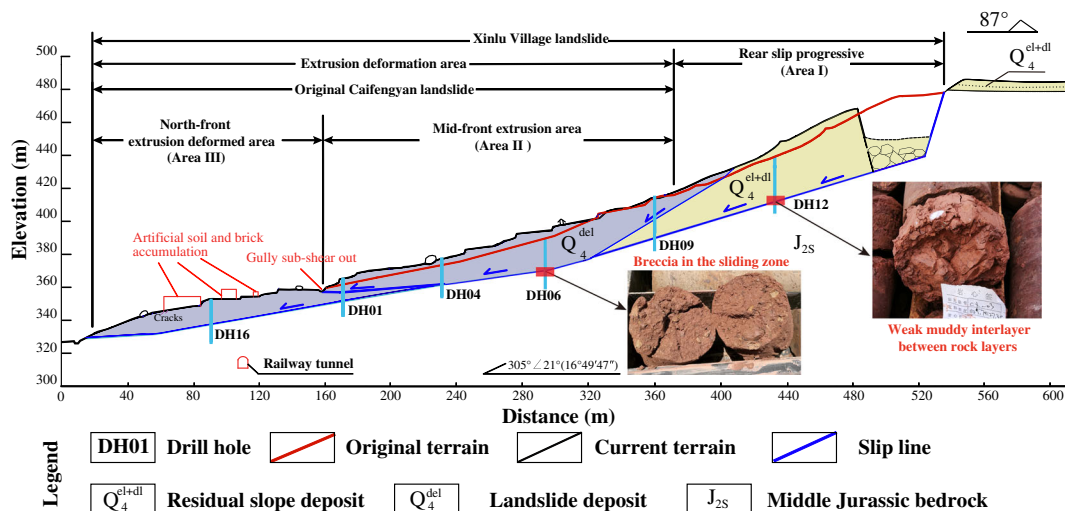$$U_i = \frac{1}{2}\gamma_w h_w l \tag{8}$$

Fig. 4 The 1-1′ section before and after the June 28, 2016, slip

Table 1 Back-calculated safety factor of the landslide before the slip

Landslide area	Shear out location	Safety factor	Stability state	Evaluation
Overall landslide (soil pushed forward by the rear rock)	West of the residential area	1.036	Stable	The rocky part on the trailing edge of the landslide actively slipped under the action of the fissure-water pressure and the sliding-surface-uplift pressure. The soil part of the leading edge slipped and sheared out at the north gully. Although the residential area was deformed, it did not slip overall. The stability state was consistent with the deformation characteristics.
	North Gully	0.952	Unstable	
Front soil part (original Caifengyan landslide)	West of the residential area	1.231	Stable	
	North Gully	1.115	Stable	

where F_s is the stability coefficient of the landslide; ψ_i is the transfer coefficient when the remaining sliding force of the i-th calculation block is transmitted to the $(i+1)$-th calculation block; R_i is the anti-sliding force of the i-th calculation block (kN/m); T_i is the slip force of the i-th calculation block (kN/m); N_i is the component force in the normal direction of the i-th calculation block sliding surface (kN/m); c_j is the standard value of the slip surface cohesion of the i-th calculation block (kPa); φ_i is the standard value of the friction angle of the sliding surface of the i-th calculation block (°); l_i is the i-th calculation block slip surface length (m); W_i is the sum of the i-th calculation block weight and the ground load (kN/m); α_i is the slip angle of the i-th calculation block (°) and is taken as negative when the slip direction is reversed; D_i is the water pressure of the i-th calculation block (kN/m); V is the water pressure on the trailing edge of the landslide (kN/m); U_i is the water pressure of the i-th calculation block slip surface (kN/m); γ_w is the unit weight of water, taken as 10 kN/m³; h_i is the height of the i-th calculation block from the groundwater level to the water level of the river (m); h_w is the height of the fracture filling water (m); β_i is the average dip of the groundwater streamline (°); and γ is the unit weight of the rock and soil (kN/m³).

For the groundwater and hydrodynamic pressure in the landslide area, we adopted the following:

(i) Observations revealed that the groundwater level in the landslide area was 0.6–38.1 m. The groundwater depth varied greatly, and the distribution was uneven. This indicated that there was no consistent or continuous groundwater level in the landslide area. Therefore, when calculating the stability of the landslide, the hydrodynamic pressure of the groundwater was not considered under storm conditions.

(ii) According to the drilling pumping test, the permeability coefficient of the sliding mass was 0.006–0.310 m/day, which indicated poor permeability. Therefore, a wet unit weight was adopted under storm conditions, and the dynamic water pressure was ignored. In addition, a large number of cracks formed after the overall slippage of the landslide, which provided paths for rainfall infiltration. In the rainy season, the sliding mass will quickly fill with water and will increase its self-weight. Hence the sliding mass was calculated to be in a saturation state under storm conditions.

(iii) The high fissure-water pressure in the trailing edge crack of the landslide and the slip surface water pressure formed by the rainfall were the direct inducers of the overall landslide on June 28, 2016. The fracture water pressure during the back-calculation was calculated as one-third of the fracture depth (Li 2016). After the initial slip on June 28, the trailing edge crack slot was open, and thus the fracture water pressure was no longer calculated.

Test values

The geotechnical parameters involved in the back-calculation process were mainly unit weight and shear strength, which were obtained as follows:

The unit weight of the sliding mass The sliding mass on the trailing edge of the landslide was the mudstone of the Mid-Jurassic Shaximiao Formation (J_{2s}). The calculated value of the rocky sliding mass was taken as the test value. The dry unit weight of the mudstone was 25.46 kN/m³, and the wet unit weight was 25.56 kN/m³. The sliding mass in the mid-front extrusion area was silty clay and gravel. The unit weight of the soil sliding mass was calculated based on the 1:1 unit weight of the silty clay and sandstone test values. The dry unit weight of silty clay and gravel was 21.81 kN/m³, and the wet unit weight was 22.11 kN/m³.

The shear strength of the sliding zone The original Caifengyan landslide had undergone an overall slip before the Xinlu Village landslide. The sliding zone was the breccia between the rock and soil and was completely connected with a thickness of 0.2–6.5 m. According to the *Technical code for building slope engineering* (Chinese National Standard), the test value of the friction angle was multiplied by an adjustment factor of 1.25 (when the content of coarse materials on site was higher than that of the test soil).

Table 2 Back-calculation results for shear strength of the sliding zone

Sliding zone	Natural shear strength Cohesive force (kPa)	Friction angle (°)	Saturation shear strength Cohesive force (kPa)	Friction angle (°)
Weak muddy interlayer between rock layers	28.00	15.00	25.0	12.8
Breccia	23.20	12.69	20.5	11.76

Table 3 Numerical calculation parameters

Operating condition	Lithology	Unit weight (kN/m³)	Elastic modulus (kPa)	Poisson's ratio	Cohesion (kPa)	Friction angle (°)
Natural conditions	Silty clay and gravel	21.81	46400	0.36	23.70	15.92
	Mudstone	25.46	5070000	0.26	423.20	36.00
	Sandstone	25.70	11500000	0.24	1678.20	44.29
	Weak muddy interlayer between rock layers	24.36	3800	0.20	28.00	15.00
	Breccia in the sliding zone	20.71	3000	0.28	23.20	12.69
	Debris of mudstone	25.46	57300	0.33	25.60	16.20
Rainstorm conditions	Silty clay and gravel	22.11	40500	0.32	22.00	13.23
	Mudstone	25.56	4030000	0.22	412.60	33.20
	Sandstone	25.80	10500000	0.20	1568.30	42.30
	Weak muddy interlayer between rock layers	24.46	3500	0.18	25.00	12.80
	Breccia in the sliding zone	20.81	2800	0.25	20.50	11.76
	Debris of mudstone	25.56	51650	0.30	24.20	14.50

The cohesive force (c) in the natural state was 22.10 kPa, and the friction angle (φ) was 12.69°, whereas under the saturated state, c was 20.50 kPa, and ϕ was 11.23°.

Empirical values

The rocky part of the landslide slid along the weak muddy interlayer, containing a small amount of gravel. The interlayers on both sides were flat and smooth. Here, c in the natural state was 28.0 kPa, and ϕ was 15.0°, whereas under the saturated state, c was 25.0 kPa, and ϕ was 12.8° (Li 2016).

Back-calculated values

According to the landslide formation characteristics and the failure mode, the pre-slip section recovery assumptions were as follows:

(i) The residual rock mass on the trailing edge of the landslide slipped overall as the rigid body;

(ii) Assuming that the front part of the landslide was a plastic body, it will swell and bulge after being squeezed and will slip overall after counteracting part of the sliding movement of the rigid body on the trailing edge;
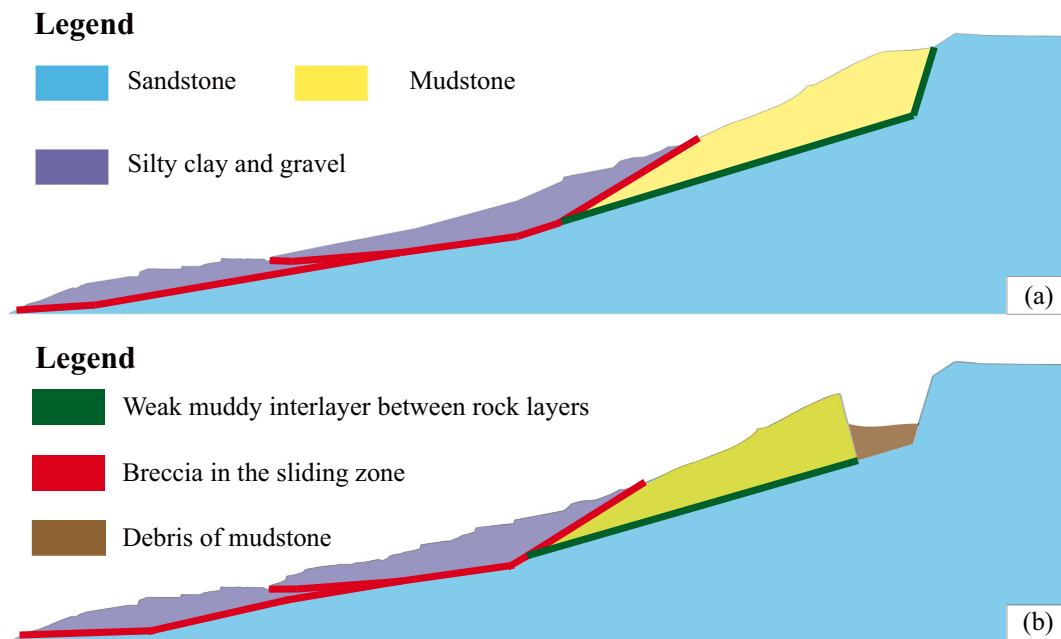

Legend

Sandstone   Mudstone

Silty clay and gravel

(a)

Legend

Weak muddy interlayer between rock layers

Breccia in the sliding zone

Debris of mudstone

(b)

Fig. 5 a Numerical model of the 1-1′ section before the slip. **b** Numerical model of the 1-1′ section after the slip

Displacement (m)

(a) Total displacement distribution under natural conditions

Displacement (m)

(b) Total displacement distribution under storm conditions

Horizon stress (kPa)

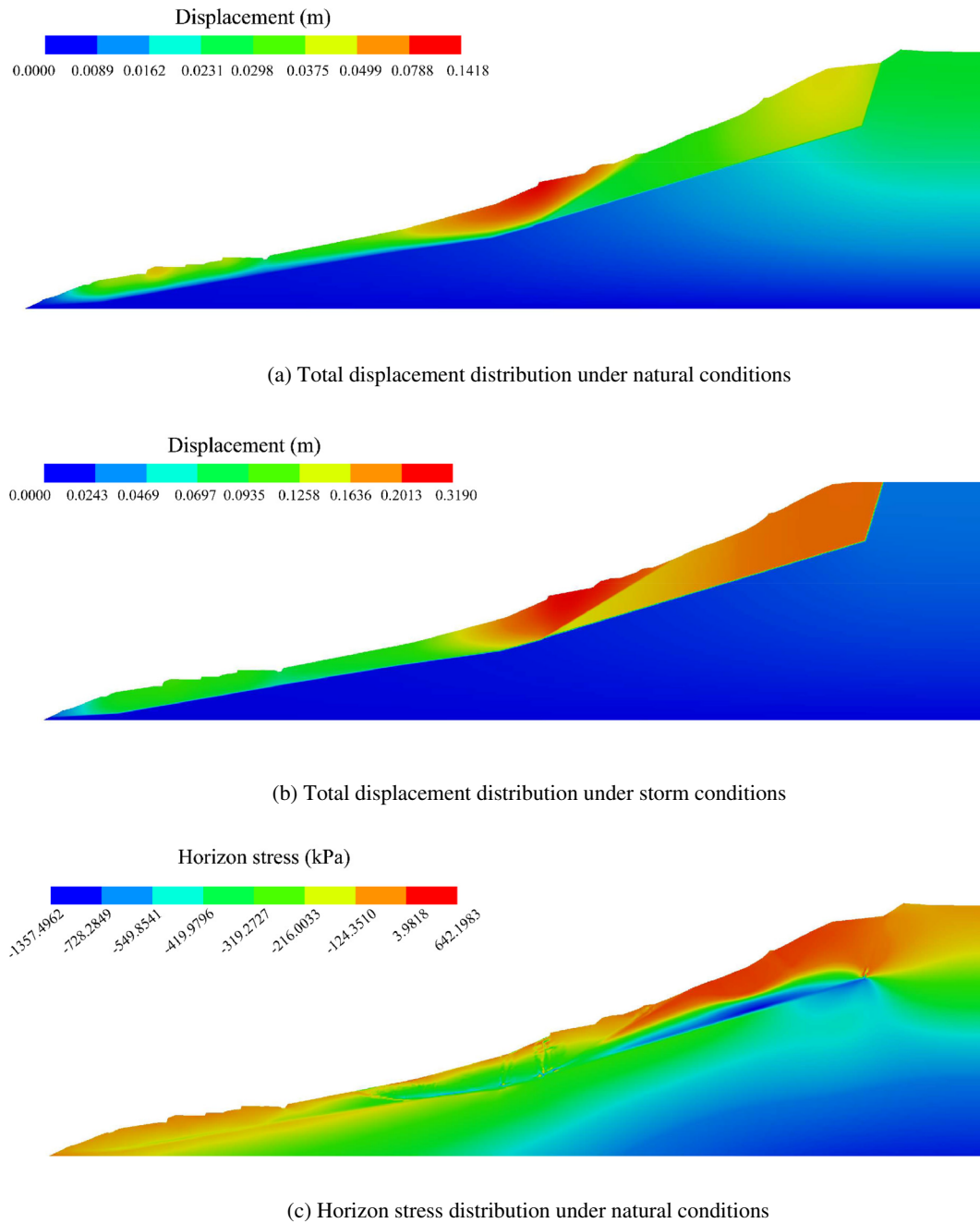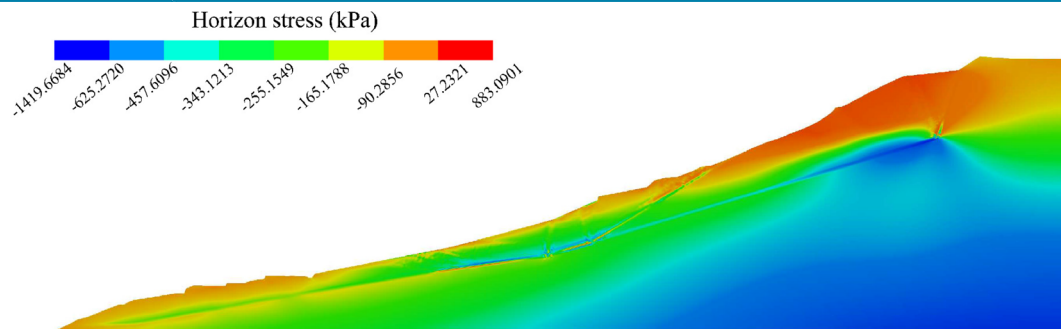(c) Horizon stress distribution under natural conditions

Fig. 6 Displacement and stress distribution under different working conditions prior to the June 28, 2016 slip (**a**). Total displacement distribution under natural conditions (**b**). Total displacement distribution under storm conditions (**c**). Horizon stress distribution under natural conditions (**d**). Horizon stress distribution under storm conditions (**e**). Vertical stress distribution under natural conditions (**f**). Vertical stress distribution under storm conditions

(iii)　The residential area in the northern front part of the land-slide was the sub-area of the extrusion deformation zone; there was no overall slip, so the section was unchanged;

(iv)　There was considerable collapsed debris in the tension crack slot on the trailing edge of the landslide, which was restored according to the principle of equal volume;

(v)　The bedrock surface of the landslide was unchanged.

　　Based on the above assumptions, the 1-1′ section was subjected to the pre-slip section recovery, and the recovery result is shown in

Fig. 4. The back-calculation of the shear strength of the restored 1-1′ section was assumed to be as follows:

(i)　The 1-1′ section was bounded by the gully. The rear part was the slip progressive area and its safety factor was 0.95–0.98. The safety factor of the deformed area at the northern front of the landslide was approximately 1.05;

(ii)　The rear rocky part slid along the soft muddy interlayer under the action of the high fracture water pressure and the surface water pressure, which were the key influential factors. Therefore, the stability factor was greater than 1.00 without the

(d) Horizon stress distribution under storm conditions
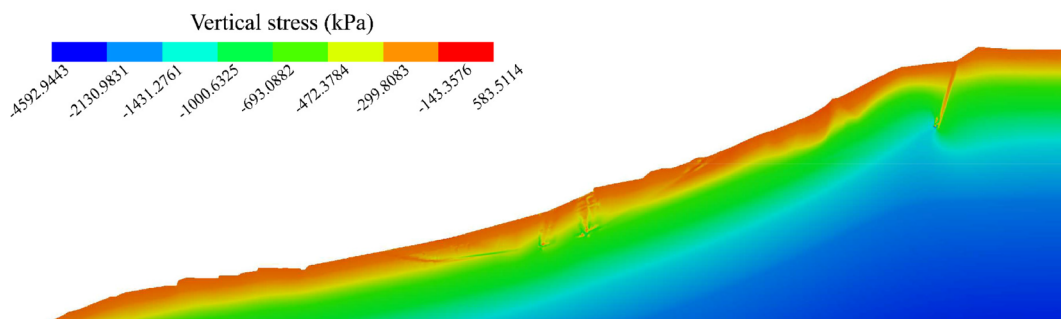
(e) Vertical stress distribution under natural conditions
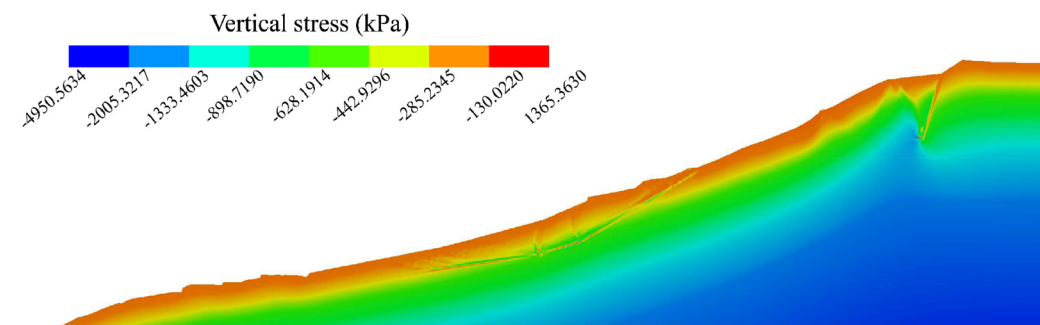
(f) Vertical stress distribution under storm conditions

Fig. 6 (continued)

fracture water pressure and the sliding-surface-uplift pressure, and the stability factor was less than 0.98 with the fracture water pressure and the sliding-surface-uplift pressure;

(iii) According to the indications of an on-site survey, the original Caifengyan landslide was in an unstable state or a basically stable state before the overall slip, with a safety factor of 1.05 to 1.10.

Based on the above assumptions, the 1-1′ section of the landslide was back-calculated. The back-calculated safety factor of the landslide before the slip is shown in Table 1, and the shear strength parameters of the sliding zone obtained from the back-calculation are shown in Table 2.

**Comprehensive selection of parameters**

According to the laboratory test, engineering analogy, and back-calculation, the required parameters for numerical calculation are shown in Table 3. The finite element method was used to simulate the landslide by the Midas GTS (Midas Geo-Technical analysis System). The Mohr–Coulomb constitutive model was used for the rock and soil involved in the numerical simulation. For the parameters of the rock mass, the elastic modulus, Poisson's ratio, and the cohesion and friction angle were obtained by the uniaxial compression test and triaxial compression test (Cai 2017). The shear strength parameters of the sliding zone were obtained by back-calculation, and the elastic modulus and Poisson's ratio for soil were determined in accordance with Lambe and Whitman (1979) and Li (2016).
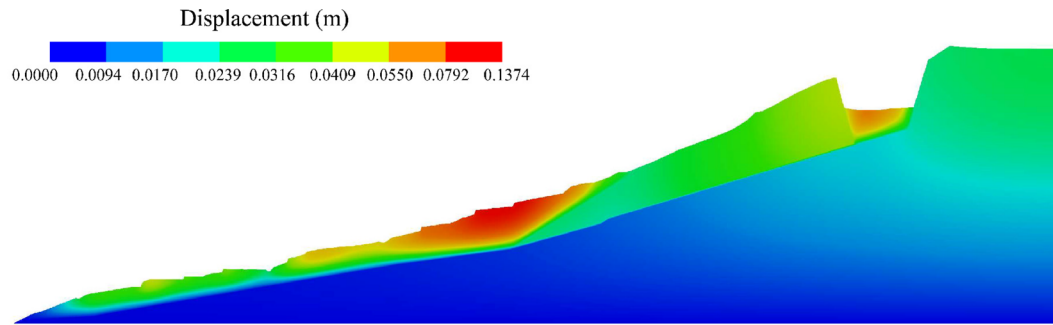
(a) Total displacement distribution under natural conditions
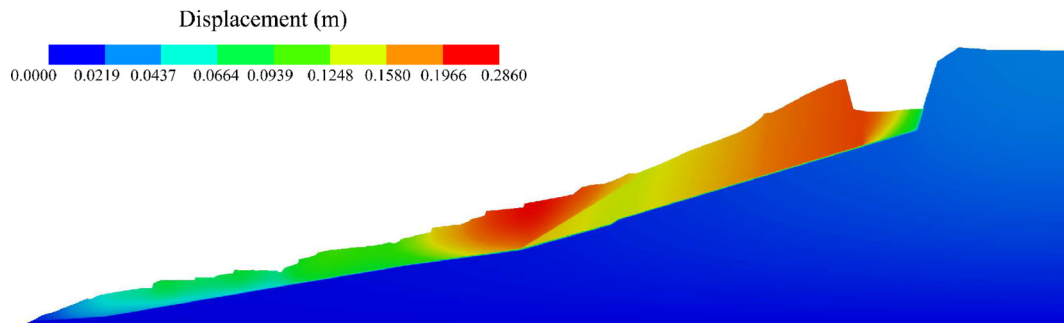
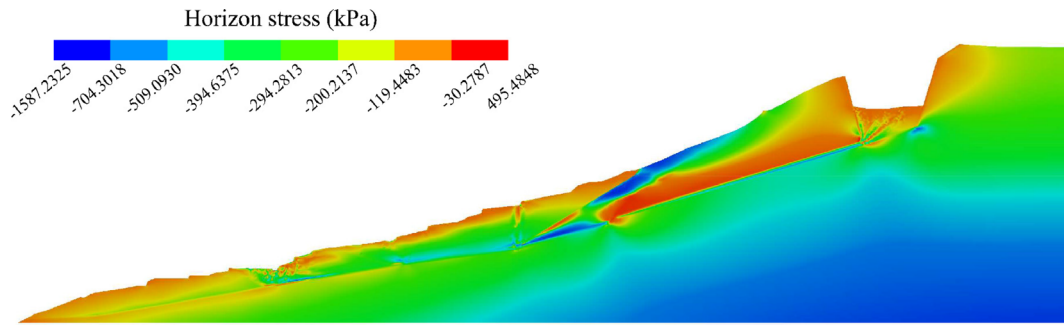(b) Total displacement distribution under storm conditions
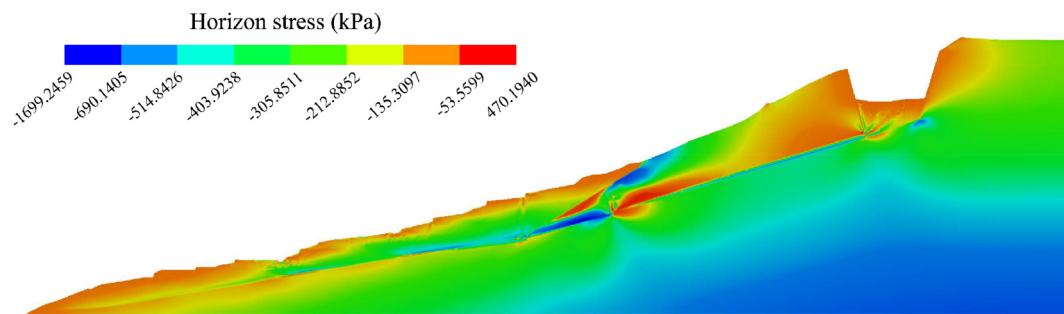
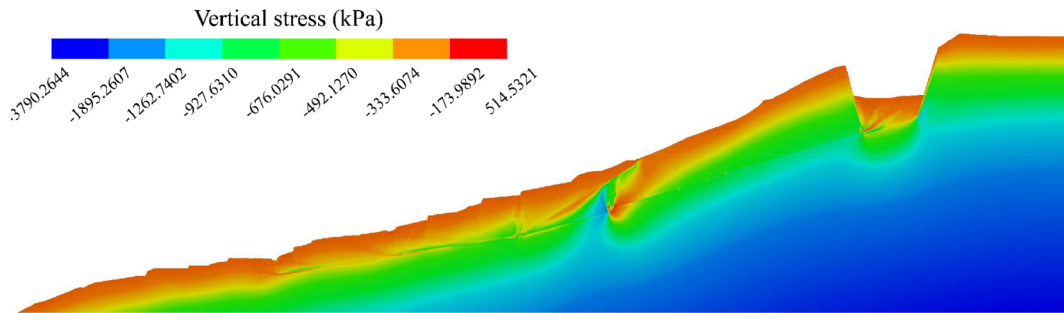(c) Horizon stress distribution under natural conditions

Fig. 7 Displacement and stress distribution under different working conditions prior to the June 28, 2016, slip (**a**). Total displacement distribution under natural conditions (**b**). Total displacement distribution under storm conditions (**c**). Horizon stress distribution under natural conditions (**d**). Horizon stress distribution under storm conditions (**e**). Vertical stress distribution under natural conditions (**f**). Vertical stress distribution under storm conditions

Numerical simulation was conducted through the c–ϕ reduction algorithm using finite elements. When the slope reached instability, the numerical non-convergence occurred simultaneously. The safety factor was then obtained by the c–ϕ reduction algorithm (Zhao et al. 2002). The back-calculated shear parameters were taken as the mechanical properties of the sliding zone. The sliding mass, sliding zone, and bedrock were all divided by the multi-node element. Among them, the sliding zone was set as a striped area with a certain thickness (Liu and

Zheng, 2006). The lateral boundary of the numerical calculation model was constrained by the horizontal displacement, and the bottom surface was constrained by the two-direction displacement. Hydrostatic pressure was applied to the trailing edge crack of the slope before the slip under storm conditions. The tension crack slot on the trailing edge of the slope after the slip was a loose deposit, so the hydrostatic pressure was no longer considered. Under storm conditions, the sliding mass was set to be in the saturated state because a large number of cracks occurred

(d) Horizon stress distribution under storm conditions

(e) Vertical stress distribution under natural conditions
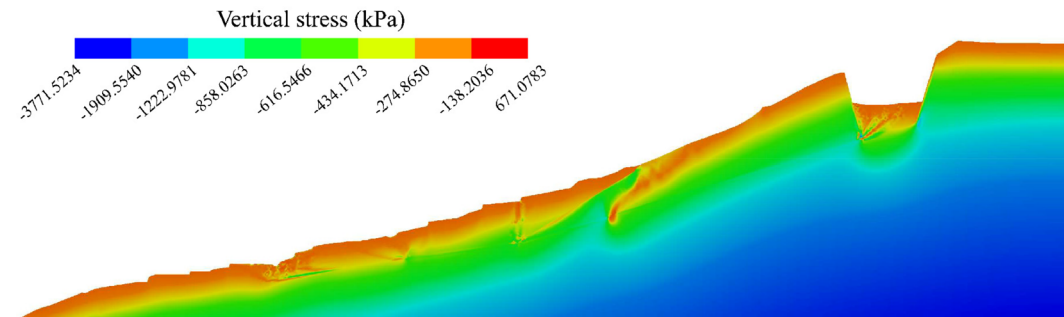
(f) Vertical stress distribution under storm conditions

Fig. 7 (continued)

in the landslide surface, and the uplift pressure would be adapted on the slide plane. Note that the location of the sliding plane was determined by on-site drilling (Fig. 2 and Fig. 4). The numerical simulation of the section 1-1′ was carried out under different sets of conditions, and the calculation models are shown in Fig. 5.

Results

The numerical calculation results were analyzed as follows.

Before the slip The total displacement and the stress distribution under different working conditions before the slip are shown in Fig. 6. The calculation results show that under natural conditions, the maximum displacement was concentrated in the connection area between the mudstone and silty clay. The front soil part did not provide sufficient anti-sliding force after the continuous rainfall. Under storm conditions, the displacement of the mudstone on the trailing edge also formed a displacement concentration zone, which was consistent with the previous analysis of the slip mechanism. Under natural conditions, the maximum displacement was 0.14 m, and the maximum displacement under storm conditions was 0.31 m, which was 2.24 times greater than that under natural conditions. The stress distribution of the section was similar under different conditions. The horizon stress was concentrated on the mudstone at the trailing edge of the sliding mass, and the vertical stress was concentrated on the surface area of the sliding mass. The maximum horizon stress under storm conditions was 1.37 times greater than that under natural conditions, and the maximum vertical stress under storm conditions was 2.33 times greater than that under natural conditions.
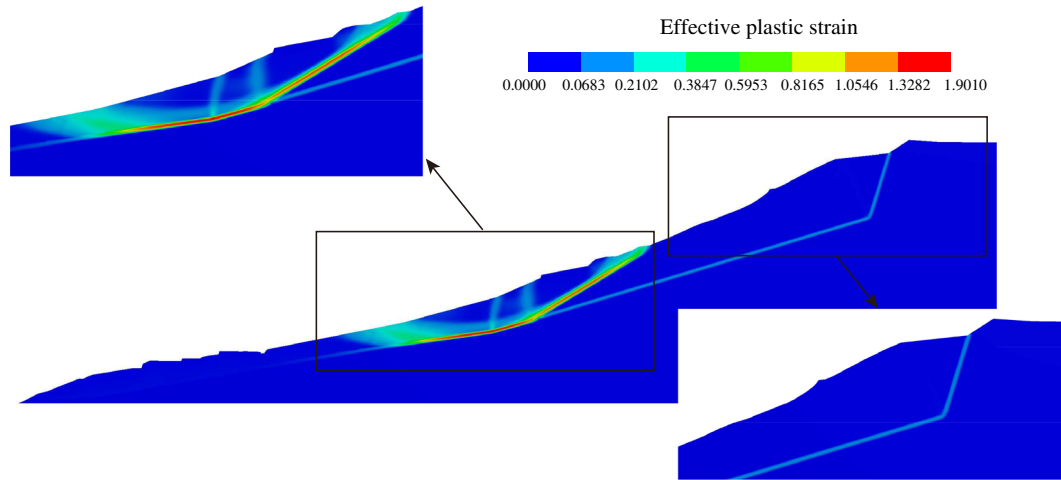
(a) Distribution of the effectiv e plastic strain before the slip under natural conditions
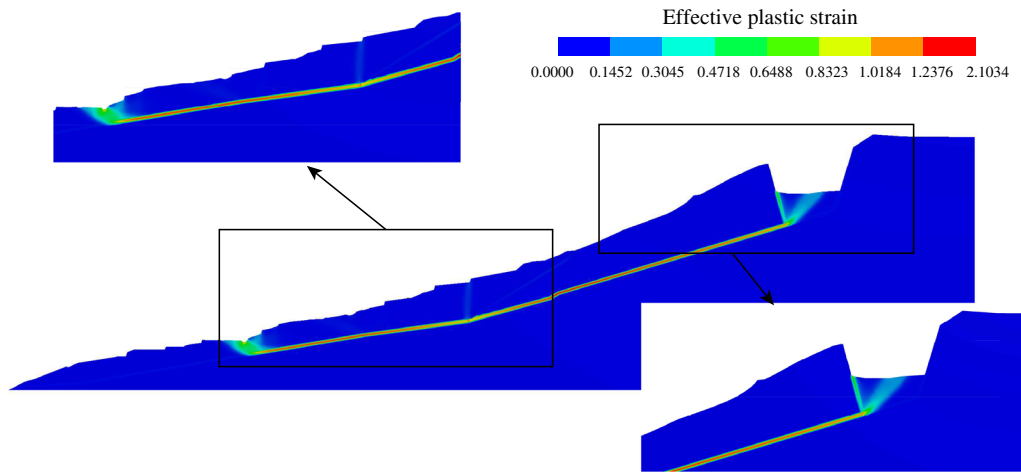(safety factor 1.05)
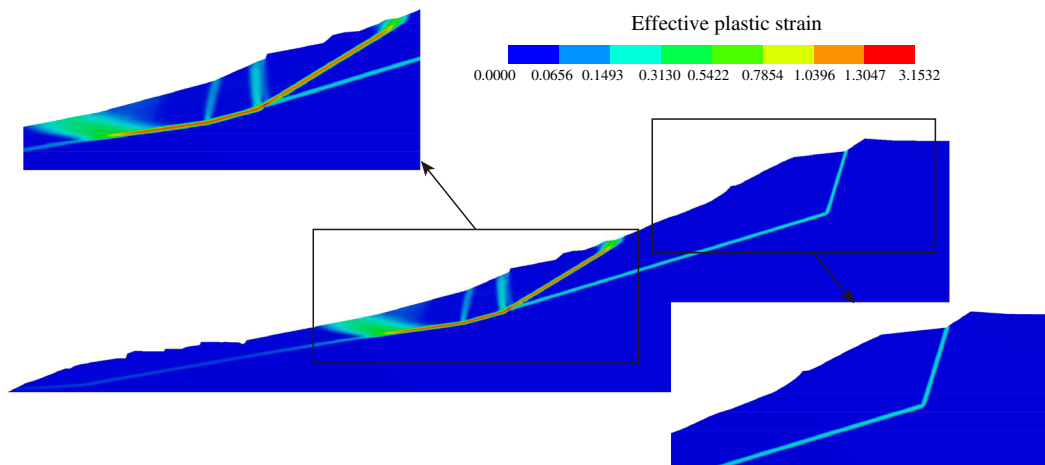
(b) Distribution of the effective plastic strain before the slip under storm conditions
(safety factor 0.97)

Fig. 8 Distribution of effective plastic strain before and after the June 28, 2016, slip (**a**). Distribution of the effective plastic strain before the slip under natural conditions (safety factor 1.05) (**b**). Distribution of the effective plastic strain before the slip under storm conditions (safety factor 0.97) (**c**). Distribution of the effective plastic strain after the slip under natural conditions (safety factor 1.03) (**d**). Distribution of the effective plastic strain after the slip under storm conditions (safety factor 0.98)

After the slip The displacement and the stress distribution under different working conditions after the slip are shown in Fig. 7. The calculation results show that under natural conditions, the maximum displacement was concentrated on the trailing edge of the original Caifengyan landslide, i.e., the connection area between the mudstone and silty clay. The maximum displacement convergence area also appeared on the front of the crack slot under storm conditions. The maximum displacement value of the section caused by heavy rain was 2.08 times greater than that under natural conditions. After slipping, stress distributions were similar under the different conditions. The horizon stress was concentrated in the interlayer of the rocky part on the trailing edge of the landslide, and there was a significant stress difference in the mudstone sliding mass. The vertical direction stress was concentrated on the surface of the sliding mass. The appearance of

the crack slot after the slip led to the stress release, and the squeezing effect of the trailing edge of the landslide was weakened. The maximum stress value of the landslide area was considerably reduced compared with that before the slip. At the same time, the sensitivity of the stress state to the heavy rain was also further reduced. Therefore, the maximum stress under storm conditions was only slightly increased compared with the maximum stress under natural conditions.

Stability analysis The safety factor of the section before and after the slip under different working conditions was obtained by the c–ϕ reduction algorithm, and the plastic zone distribution before the slip is shown in Fig. 8(a, b). The distribution of the plastic deformation zone under different working conditions was similar and was connected along the sliding zone on the trailing edge of

(c) Distribution of the effective plastic strain after the slip under natural conditions
(safety factor 1.03)
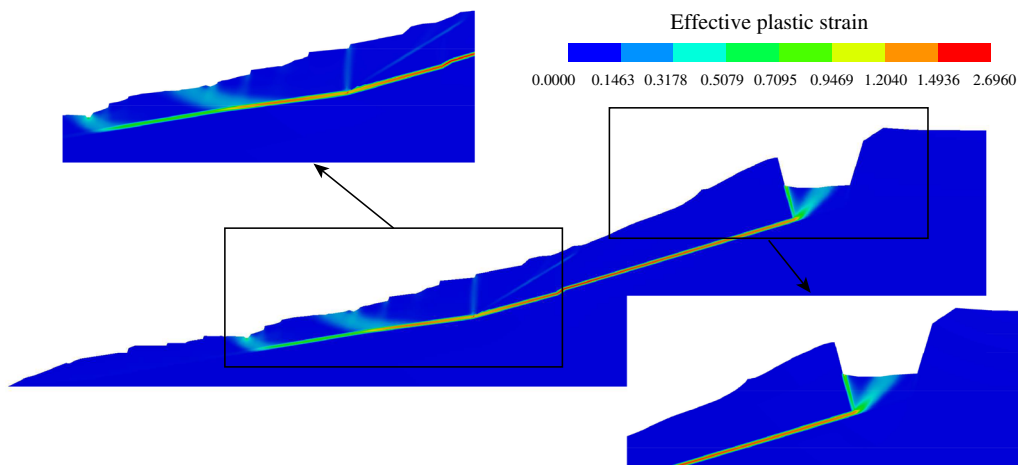
(d) Distribution of the effective plastic strain after the slip under storm conditions
(safety factor 0.98)

Fig. 8 (continued)

the soil part (original Caifengyan landslide). Under storm conditions, the plastic strain zone of the section expanded, and the safety factor decreased from 1.05 to 0.97. The plastic zone distribution after the slip is shown in Fig. 8(c, d). The distribution of the plastic deformation area of the section under different working conditions was also similar, and the plastic strain zone connected from the crack slot to the shear out of the soil part. Under the storm conditions, the plastic strain zone further expanded, and the safety factor decreased from 1.03 to 0.98.

Discussion

There were several similar situations in the numerical analysis before and after the slip. Firstly, the maximum displacement of the section under storm conditions was approximately 2 times that under natural conditions, both before and after the slip. The maximum displacement of the section was concentrated on the trailing edge of the original Caifengyan landslide, and under the storm conditions, the maximum displacement

concentrated area extended to the mudstone part. Secondly, the horizontal stress was concentrated in the mudstone part, and a considerable stress difference formed in the sliding zone of the mudstone part. This promoted the instability and slip of the landslide. Thirdly, the vertical stress was concentrated on the surface portion of the sliding mass.

However, the stress state changed because of the change in surface morphology after the slip. Before the slip, the stress state of the section was sensitive to rainfall. The maximum horizontal stress of the section under storm conditions was 1.37 times that under natural conditions, and the maximum vertical stress under storm conditions was 2.33 times that under natural conditions. After the slip, due to the occurrence of the crack slot, the integrity of the landslide was destroyed and the stress was greatly reduced. At the same time, the sensitivity to heavy rain was further reduced. In addition, under storm conditions, the section was in an unstable state before and after the slip. The numerical calculation results of the landslide were basically consistent with the macroscopic judgment of landslide stability.

We performed the same analysis and calculations on the nine sections in the Xinlu Village landslide (Fig. 2). After the slip, the landslide was in a stable state under natural conditions, and the northern front part of the landslide was unstable under storm conditions. This is because rainfall quickly infiltrated through the existing deformation cracks into the landslide debris, increasing the self-weight of the sliding mass, further reducing the strength of the weakened sliding zone, and deteriorating the stability of the landslide after the slip. Under the action of the hydrostatic pressure and the sliding-surface-uplift pressure, the landslide is likely to slip again.

Conclusions

Due to continuous rainfall in the landslide area, high fissure-water pressure on the trailing edge and sliding-surface-uplift pressure were formed. The shear strength of the muddy interlayer was reduced, resulting in slippage of the rocky part of the landslide. Under the compression of the rocky part, the soil part directly slipped, and the debris flow was triggered at the same time. The landslide failure mode was determined to be a slumping slide.

To ensure the accuracy of the numerical calculation, the typical section before the slip was restored on the basis of macroscopic qualitative evaluation, and the mechanical parameters of the sliding zone were back-calculated based on the laboratory test. The finite element method was used to analyze the section before and after the slip under different working conditions. The displacement, stress, effective plastic strain distribution, and the safety factor obtained by numerical calculation were consistent with qualitative evaluation, thus verifying the rationality of the landslide formation mechanism and failure mode analysis.

The Xinlu Village landslide, after the initial sliding, was in a peristaltic stage. The weak sliding zone was completely connected, and the landslide could be in an unstable state under storm conditions.

Compliance with ethical standards

Disclaimer This paper is a product of the study on the Long-term Strength Weakening Law and Protection Measures of the Yangtze River Water Level in the Chongqing Reservoir Area of the Three Gorges.

References

Crosta GB, Frattini P (2008) Rainfall-induced landslides and debris flows. Hydrol Process 22(4):473–477

Cai MF (2017) Rock mechanics and engineering (Second Edition). Beijing Science Press **(in Chinese)**

Cheng D, Cui Y, Su F, Jia Y, Choi CE (2018) The characteristics of the Mocoa compound disaster event, Colombia. Landslides 15(6):1223–1232

Clague J, Stead D (2012) Landslides-types, Mechanisms and Modeling. Cambridge University Press

Gao Y, Yin YP, Li B, Feng Z, Wang WP, Zhang N, Xing AG (2017) Characteristics and numerical runout modeling of the heavy rainfall-induced catastrophic landslide-debris flow at Sanxicun, Dujiangyan, China, following the Wenchuan Ms 8.0 earthquake. Landslides 14(4):1361–1374

Hungr O, Evans SG (2004) The occurrence and classification of massive rock slope failure. Felsbau—Rock and Soil Engineering 22:16–23

Irfan M, Uchimura T, Chen YL (2017) Effects of soil deformation and saturation on elastic wave velocities in relation to prediction of rain-induced landslides. Eng Geol 230:84–94

Lambe TW, Whitman RV (1979) Soil mechanics: SI version. Wiley, New York

Liao ZH, Hong Y, Wang J, Fukuoka H, Sassa K, Karnawati D, Fathani F (2010) Prototyping an experimental early warning system for rainfall-induced landslides in Indonesia using satellite remote sensing and geospatial datasets. Landslides 7(3):317–324

Li GX (2016) Advanced in soil mechanics (Second Edition). Beijing: Tsinghua University Press **(in Chinese)**

Li CR, Wang M, Liu K (2018) A decadal evolution of landslides and debris flows after the Wenchuan earthquake. Geomorphology. 323:1–12

Lin F, Wu LZ, Huang RQ, Zhang H (2018) Formation and characteristics of the Xiaoba landslide in Fuquan, Guizhou, China. Landslides 15:669–681

Ling H, Ling HL, Li L, Kawabata T (2010) Centrifuge modeling of slope failures induced by rainfall. Proc 7th Int Conf on Physical Modelling in Geotechnics. 1131–1136

Liu MW, Zheng YR (2006) Determination methods of multi-slip surfaces landslide based on strength reduction FEM. Chin J Rock Mech Eng 08:1544–1549 **(in Chinese)**

Rahimi A, Rahardjo H, Leong EC (2011) Effect of antecedent rainfall patterns on rainfall-induced slope failure. J Geotech Geoenviron 137(5):483–491

Ren F, Ma GW, Wang Y, Fan LF (2016) Pipe network model for unconfined seepage analysis in fractured rock masses. International Journal of Rock Mechanics & Mining Sciences 88:183–196

Technical code for building slope engineering (2013) The National Standards Compilation Group ofPeople's Republic of China. China Planning Press, Beijing **(in Chinese)**

Wen HJ, Zhang YY, Fu HM, Xie P, Hu J (2018) Research status of instability mechanism of rainfall-induced landslide and stability evaluation methods. China Journal of Highway and Transport 31(02):15–29+96 **(in Chinese)**

Wu W (2015) Recent advances in modeling landslides and debris flows. Springer

Wang LQ, Yin YP, Huang BL, Zhang ZH, Wei YJ (2019) Formation and characteristics of Guang'an Village landslide in Wuxi, Chongqing, China. Landslides 16:127–138

Yin YP, Cheng YL, Liang JT, Wang WP (2016) Heavy-rainfall-induced catastrophic rockslide-debris flow at Sanxicun, Dujiangyan, after the Wenchuan Ms 8.0 earthquake. Landslides 13(1):9–13

Zhang M, Yin YP, Huang BL (2015) Mechanisms of rainfall-induced landslides in gently inclined red beds in the eastern Sichuan Basin, SW China. Landslides 12(5):973–983

Zhao SY, Zheng YR, Shi WM, Wang JL (2002) Analysis on safety factor of slope by strength reduction FEM. Chinese Journal of Geotechnical Engineering 03:343–346 **(in Chinese)**

Zhao LH, Zuo S, Deng DP, Han Z, Zhao B (2018) Development mechanism for the landslide at Xinlu Village, Chongqing, China. Landslides 15(10):2075–2081

L. Wang
Faculty of Engineering,
China University of Geosciences,
Wuhan, 430074, China

L. Wang · Z. Zhang · P. Zhao · M. Hu
No.208 Hydrogeology and Engineering Geology Team of Chongqing Bureau of Geology and Minerals Exploration,
Chongqing, 400700, China

Y. Yin (✉) **· Y. Wei**
China Institute of Geological Environment Monitoring,
Beijing, 100081, China
Email: cug22017@163.com

B. Huang
Hubei Key Laboratory of Disaster Prevention and Mitigation,
China Three Gorges University,
Yichang, 443002, China